Catal Lett (2009) 129:170–180
DOI 10.1007/s10562-008-9786-9

# Hydrodealkylation of $C_9^+$ Heavy Aromatics to BTX over Zeolite-Supported Nickel Oxide and Molybdenum Oxide Catalysts

**Qunbing Shen · Xuedong Zhu · Jiaojiao Dong · Zibin Zhu**

Received: 17 September 2008 / Accepted: 16 November 2008 / Published online: 9 January 2009


**Abstract** Two series of catalysts with nickel oxide or molybdenum oxide as the active component and with different zeolites as supports were prepared by incipient wetness impregnation method, and their structural properties and acidity were characterized by means of XRD, $H_2$-TPR, $N_2$ adsorption and desorption, FTIR spectrum of adsorbed pyridine and $NH_3$-TPD. The catalytic activity of the prepared materials was investigated for the hydrodealkylation of commercial $C_9^+$ heavy aromatics to BTX. The results show that the catalytic performance is greatly influenced by the specific surface area, the acidity and the interaction between zeolite and metal oxide, and little affected by the pore diameter of catalysts. For NiO catalysts, the samples with the moderate interaction between zeolite and NiO exhibit the relatively high selectivity of BTX. And for $MoO_3$ catalysts, the presence of the molybdenum species associated with Brønsted acid site causes the remarkable reduction of selectivity. The presence of Brønsted acid sites, the growth of the strength of Lewis acid sites and the increase of acid amount and the specific surface area can all enhance the conversion of $C_9^+$ aromatics. Finally, compared with other zeolites, the HMCM-56 catalysts show the excellent overall catalytic performance with the yield of BTX more than 60 mol%, whether using NiO or $MoO_3$ as the active component.

Q. Shen · X. Zhu · J. Dong · Z. Zhu (✉)
Engineering Research Center of Large Scale Reactor Engineering and Technology, East China University of Science and Technology, 200237 Shanghai, China
e-mail: zhuzb@ecust.edu.cn

X. Zhu
State Key Laboratory of Chemical Engineering, East China University of Science and Technology, 200237 Shanghai, China

**Keywords** BTX · $C_9^+$ heavy aromatics · Hydrodealkylation · Zeolite · Nickel oxide · Molybdenum oxide

## 1 Introduction

With more large aromatics complex processes put into production, the throughput of by-product heavy aromatics which have more than nine carbon numbers will be increased to a great extent. Heavy aromatics are of low industrial value and are usually consumed as fuel, which wastes the aromatic resources and has been restricted by new environmental regulations. Meanwhile, as the three basic aromatic starting reactants, benzene, toluene, and xylenes (BTX) are in great demand for the manufacture of monomer for polyesters and phthalates, engineering plastics, pharmaceuticals, etc. But there is a large mismatch between the supply and the market demand. Catalytic hydrodealkylation of $C_9^+$ heavy aromatics can be employed to produce BTX with its advantages of low hydrogen consumption, high conversion and high selectivity. So many big companies and research institutes devote their attention to the catalytic hydrodealkylation technology and several commercial processes such as TAC9, ZEOLYST/SK, Detol and etc., have been developed. Now the major aim of investigation is the development of new types of catalysts.

Catalysts employed in hydrodealkylation of $C_9^+$ heavy aromatics or alkylaromatics are mainly transitional metal or transitional metal oxide catalysts supported on oxides [1–5] or zeolites. Hydrodealkylation over zeolite catalysts occurs at relatively lower temperature and helps to restraining the deactivation of catalysts. So recently studies on zeolite catalysts become the principal direction and

some catalysts have been developed [6–13]. The involved zeolite supports include ZSM-5, Beta, mordenite, Y, MCM-22 and etc., but in most literatures the influence of various zeolies on the catalytic performance is scarcely studied. And in most catalysts noble metals such as Pt, Re, and Pd are used as active components, which increases the production cost. In addition, many of investigated feeds are model aromatic compounds, such as ethylbenzene, trimethylbenzene, and ethyltoluene, and not commercial $C_9^+$ heavy aromatics with more $C_{10}$ ingredients, which limits the application of hydrodealkylation catalysts.

In the current paper, the main objective is to investigate the effect of different zeolites on the structural properties and acidity of zeolite-supported metal oxide catalysts and their catalytic performance in hydrodealkylation of commercial $C_9^+$ heavy aromatics. For this purpose, two series of catalysts with cheap NiO or $MoO_3$ as the active component and with different zeolites as supports were prepared by incipient wetness impregnation method and characterized by means of XRD, $H_2$-TPR, $N_2$ adsorption and desorption, FTIR spectrum of adsorbed pyridine and $NH_3$-TPD. And the correlation between the structural properties and acidity of the catalysts and their catalytic activity was discussed.

## 2 Experimental

### 2.1 Catalyst Preparation

HZSM-5 and H$\beta$ zeolites were commercial shaped samples supplied by the Catalyst Plant of Nankai University. Zeolite KL (Refinery of Sinopec's Jinling Petrochemical Corp., Ltd.), Na-MCM-22 (Jilin University), and Na-MCM-56 (Jilin University) were converted into the acid form by ion exchange with an aqueous solution of $NH_4NO_3$ at 85 °C for 6 h and ulterior calcination at 540 °C for 6 h. Then the H-type zeolites were shaped by adding an alumina binder, kneading, and extrusion. Nickel oxide or molybdenum oxide catalysts supported on above H-type zeolites with the loading of 15 wt% were prepared by incipient wetness impregnation method. The zeolite supports with sizes ranging from 20 to 40 meshes were impregnated with an aqueous solution of $Ni(NO_3)_2 \cdot 6H_2O$ or $(NH_4)_6Mo_7O_{24} \cdot 4H_2O$ at room temperature for 24 h. Then the samples were dried at 120 °C and calcined in air at 500 °C for 6 h. Here the NiO or $MoO_3$ loading represents the mass ratio of NiO or $MoO_3$ to dry zeolite support.

### 2.2 Catalyst Characterization

X-ray diffraction characterization was performed in a Rigaku D/max 2550 VB/PC X-ray diffractometer with $CuK_\alpha$ radiation. BET specific surface area, pore volume and pore diameter of the catalysts were determined by $N_2$ adsorption and desorption data acquired through a Micromeritics ASAP 2020 instrument.

A Micromeritics AutoChem 2920 system was used to carry out $H_2$-TPR measurements of the catalysts. Thus, the samples were degassed under Ar flow (30 mL $min^{-1}$) at 300 °C for 2 h and cooled down to room temperature. Then the samples were subjected to reduction under 10% $H_2$/Ar (v/v) flow (30 mL $min^{-1}$) and heating rate of 10 °C $min^{-1}$. The $H_2$ consumption was measured by a TCD.

A Nicolet NEXUS 470 FTIR spectrometer was used to follow the pyridine adsorbed on the acid sites of the catalysts. To do this, self-supported wafers were pretreated under vacuum at 300 °C for 4 h and then cooled down to room temperature. After acquisition of the background spectrum, pyridine vapor was admitted to the cell until equilibrium was reached. The samples were then desorbed at 100, 150, 200, 250, and 300 °C with spectra acquisition.

$NH_3$-TPD measurements were carried out in a PX200A TPD equipment with a TC detector made by China Tianjin Golden Eagle Technology Co., Ltd. Before $NH_3$ adsorption, the samples were pretreated in a He flow (30 mL $min^{-1}$) at 500 °C for 1 h, then cooled down to less than 150 °C and saturated with a 5% $NH_3$/He (v/v) mixture. Finally the samples were purged with a He stream for desorption at a heating rate of 10 °C $min^{-1}$ until a constant base line was obtained.

### 2.3 Catalytic Test

The catalytic performance in hydrodealkylation of $C_9^+$ heavy aromatics was measured in a continuous high-pressure fixed-bed stainless steel microreactor with an inner diameter of 12 mm and 1.5 g of catalyst was loaded. A cooler and a gas–liquid separator were also included in the experimental system. The liquid feed flow, the $H_2$ flow and the total pressure were controlled with a high-pressure piston pump, a mass-flow controller and a back-pressure regulator, respectively. The feed and liquid products were quantitatively analyzed in an Agilent 6820 GC with a HP-5MS capillary column and a flame ionization detector. The feed of commercial $C_9^+$ heavy aromatics which consisted of 59.82 wt% of $C_9$ aromatics, 37.03 wt% of $C_{10}$ aromatics and 3.16 wt% of $C_{10}^+$ aromatics was heavy reformate supplied by Refinery of Sinopec's Jinling Petrochemical Corp., Ltd. And $H_2$ (99.99%) was supplied by Shanghai Donghui Gas Corporation.

Conversion of $C_9^+$ heavy aromatics [$X(C_9^+)$], selectivity of BTX [$S$(BTX)] and yield of BTX [$Y$(BTX)] were calculated as follows:

$$X\left(C_9^+\right) = \frac{n_f(C_9^+) - n_p(C_9^+)}{n_f(C_9^+)} \times 100\%$$

$$S(\mathrm{BTX}) = \frac{n_p(\mathrm{BTX}) - n_f(\mathrm{BTX})}{n_f(C_9^+) - n_p(C_9^+)} \times 100\%$$

$$Y(\mathrm{BTX}) = X\left(C_9^+\right) \times S(\mathrm{BTX})$$

where $n_f(C_9^+)$ = mole of $C_9^+$ aromatics in the feed (mol); $n_p(C_9^+)$ = mole of $C_9^+$ aromatics in liquid products (mol); $n_f$(BTX) = mole of BTX in the feed (mol); $n_p$(BTX) = mole of BTX in liquid products (mol).

## 3 Results and Discussion

### 3.1 Catalyst Characterization

#### *3.1.1 XRD*

XRD patterns of nickel oxide catalysts with different zeolites as supports are shown in Fig. 1. It can be found that the characteristic diffraction peaks of NiO crystal at $2\theta$ = 37.2°, 43.3°, and 62.9° all appear for each of above five catalysts, which indicates that the active component of nickel exists as NiO crystallite in these catalysts. But the strength of the peaks differs depending on the zeolite support. So the interaction between NiO and zeolite, i.e., the dispersion state of NiO on the surface of zeolite, is affected by different zeolites. In addition, the characteristic diffraction peaks of involved zeolites also appear distinctly in Fig. 1, which indicates that the crystal structures of zeolite supports are not destroyed after impregnation and calcination.

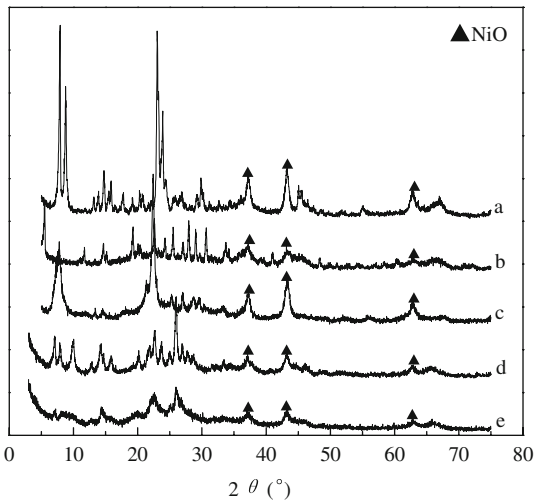


**Fig. 1** XRD patterns of zeolite-supported nickel oxide catalysts: (*a*) NiO/HZSM-5; (*b*) NiO/HL; (*c*) NiO/H$\beta$; (*d*) NiO/HMCM-22 and (*e*) NiO/HMCM-56

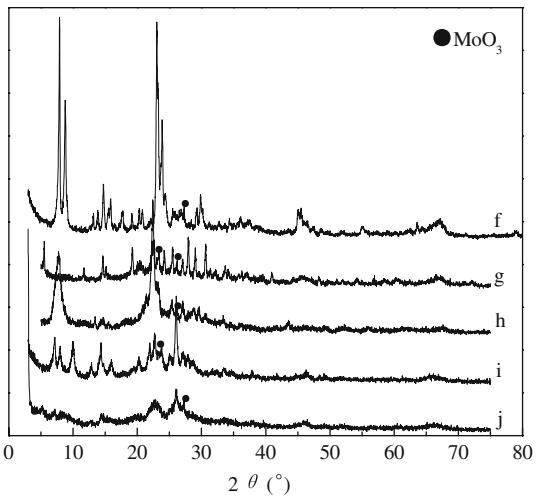


**Fig. 2** XRD patterns of zeolite-supported molybdenum oxide catalysts: (*f*) $MoO_3$/HZSM-5; (*g*) $MoO_3$/HL; (*h*) $MoO_3$/H$\beta$; (*i*) $MoO_3$/HMCM-22 and (*j*) $MoO_3$/HMCM-56

From the XRD patterns shown in Fig. 2, the characteristic diffraction peaks of $MoO_3$ crystal can be observed in part for these zeolite-supported molybdenum oxide catalysts, which indicates that the active component of molybdenum exists as $MoO_3$ crystallite in them. For $MoO_3$/HZSM-5 and $MoO_3$/HMCM-56, the diffraction peak appears at $2\theta$ = 27.3° corresponding to the {0 2 1} reflection of $MoO_3$. And for $MoO_3$/HL, the diffraction peaks at $2\theta$ = 23.4° and 26.2° which are ascribed to the {1 1 0} and {0 4 0} reflections of $MoO_3$, respectively, can be detected. The peak at $2\theta$ = 26.2° which is ascribed to the {0 4 0} reflection of $MoO_3$ is found for $MoO_3$/H$\beta$ while the peak at $2\theta$ = 23.4° corresponding to the {1 1 0} reflection of $MoO_3$ is observed for $MoO_3$/HMCM-22. As indicated for above NiO catalysts, the crystal structures of zeolites involved in these $MoO_3$ catalysts are not destroyed similarly.

#### *3.1.2 $H_2$-TPR*

Temperature-programmed reduction of hydrogen ($H_2$-TPR) was employed to determine the reduction performance of zeolite-supported nickel oxide and molybdenum oxide catalysts described in Figs. 3 and 4, respectively, so as to investigate further the interaction status between NiO or $MoO_3$ and zeolite.

From Fig. 3, for the NiO/HZSM-5 sample, three reduction peaks appear at 388, 500, and 570 °C, which indicates the presence of three different nickel species. The peak at 388 °C can be assigned to the reduction of NiO particles with normal crystal size, and the peak at 500 °C can be due to the reduction of NiO particles interacting with HZSM-5 and not easy to be reduced. Finally, the peak at 570 °C may be associated with the reduction of nickel

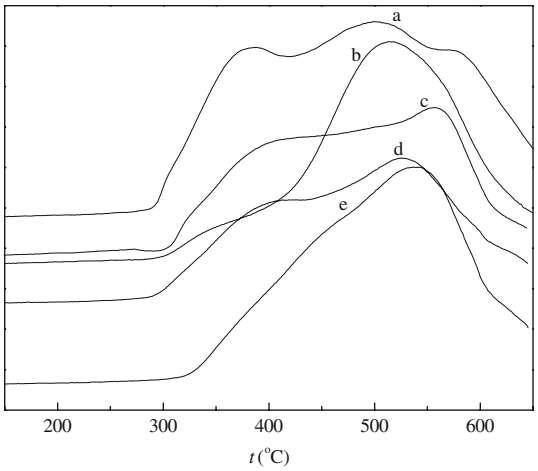


**Fig. 3** $H_2$-TPR profiles of zeolite-supported nickel oxide catalysts: (*a*) NiO/HZSM-5; (*b*) NiO/HL; (*c*) NiO/H$\beta$; (*d*) NiO/HMCM-22 and (*e*) NiO/HMCM-56

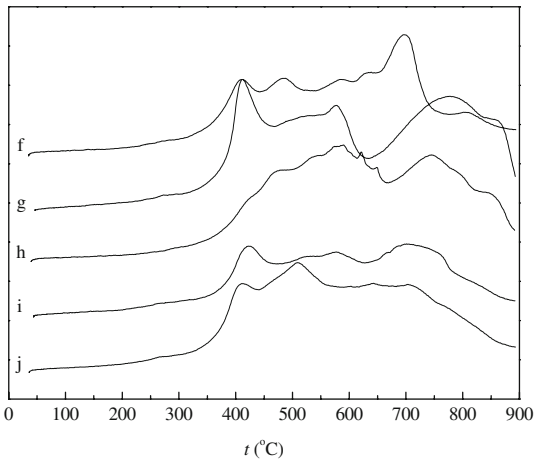


**Fig. 4** $H_2$-TPR profiles of zeolite-supported molybdenum oxide catalysts: (*f*) $MoO_3$/HZSM-5; (*g*) $MoO_3$/HL; (*h*) $MoO_3$/H$\beta$; (*i*) $MoO_3$/HMCM-22 and (*j*) $MoO_3$/HMCM-56

species located in the framework of HZSM-5 and hard to be reduced [14]. Two peaks at 340 and 514 °C corresponding to the reduction of relatively big NiO particles and nickel species interacting with HL and not easy to be reduced, respectively, are observed in the TPR profile of NiO/HL. For the NiO/H$\beta$ sample, the peak at about 400 °C can be due to the reduction of NiO particles with normal crystal size, whereas the peak at 556 °C may be assigned to the reduction of nickel species located in the framework of H$\beta$ and hard to be reduced [15]. The NiO/HMCM-22 sample also shows two peaks at about 400 and 526 °C corresponding to the reduction of NiO particles with normal size and nickel species interacting with HMCM-22 and not easy to be reduced, respectively. Only one peak at 537 °C appears in the TPR profile of NiO/HMCM-56, and it can be assigned to the reduction of NiO particles interacting with HMCM-56 and not easy to be reduced.

So the $H_2$-TPR results reveal that nickel species exists only as NiO crystallite in these nickel oxide catalysts, though the interaction status between NiO and zeolite differs depending on the zeolite support. And this just accords with the XRD results.

It can be seen from Fig. 4 that there are several molybdenum species in each of above $MoO_3$ catalysts. Generally, the reduction process of $MoO_3$ in $H_2$ atmosphere follows the order: $MoO_3 \rightarrow MoO_2 \rightarrow Mo$ [16]. For $MoO_3$/HZSM-5 prepared by impregnation method, the possible molybdenum species [17] includes $MoO_3$ located on the outer zeolite surface and existing as a monolayer dispersion state, $MoO_3$ located on the outer zeolite surface and existing as an aggregate state, the molybdenum species located in the channels of HZSM-5 zeolite and associated with Brønsted acid site, and $Al_2(MoO_4)_3$, i.e., the molybdenum species interacting strongly with the framework Al in tetrahedral coordination. In the present work, five reduction peaks appear in the TPR profile of $MoO_3$/HZSM-5. Firstly, the peak at 413 °C can be assigned to the reduction of molybdenum species located on the outer zeolite surface and existing as a monolayer dispersion state from $MoO_3$ to $MoO_2$ (process A) and the peak at 606 °C can be due to the further reduction of this species from $MoO_2$ to Mo (process B). Then the peak at 486 °C can be assigned to the reduction of molybdenum species located on the outer zeolite surface and existing as an aggregate state from $MoO_3$ to $MoO_2$ (process C) and the peak at

**Table 1** $H_2$-TPR results for zeolite-supported molybdenum oxide catalysts

| Peak | $MoO_3$/HL | | $MoO_3$/H$\beta$ | | $MoO_3$/HMCM-22 | | $MoO_3$/HMCM-56 | |
|---|---|---|---|---|---|---|---|---|
| | *t* (°C) | Reduction process | *t* (°C) | Reduction process | *t* (°C) | Reduction process | *t* (°C) | Reduction process |
| 1 | 419 | A | 415 | A | 418 | A | 414 | A |
| 2 | 505 | C | 473 | C | 497 | C | 501 | C |
| 3 | – | – | 545 | F | – | – | – | – |
| 4 | 577 | B | 603 | B | 576 | B | 629 | B |
| 5 | 770 | D | 750 | D + G | 705 | D | 722 | D |
| 6 | 864 | E | 850 | E | – | – | – | – |

696 °C can be due to the further reduction of this species from $MoO_2$ to Mo (process D). Finally, the peak at 821 °C can be ascribed to the reduction of $Al_2(MoO_4)_3$ (process E). Accordingly, the possible ascription of reduction peaks for other four $MoO_3$ catalysts is listed in Table 1. Process F represents the reduction of molybdenum species located in the channels of zeolite and associated with Brønsted acid site from $MoO_3$ to $MoO_2$ and process G represents the further reduction of this species from $MoO_2$ to Mo.

For $MoO_3$/HZSM-5, $MoO_3$/HL, and $MoO_3$/H$\beta$ catalysts, the $H_2$-TPR results reveal the presence of $Al_2(MoO_4)_3$ species, but the diffraction peaks of $Al_2(MoO_4)_3$ crystal cannot be detected in their XRD patterns. This indicates that the $Al_2(MoO_4)_3$ species is well dispersed in the framework of zeolite and very small in size. In the present work, compared with other $MoO_3$ catalysts, the molybdenum species associated with Brønsted acid site exists only in the $MoO_3$/H$\beta$ sample, which indicates the presence of Brønsted acid site in it. And this will be confirmed by the measurements of acidity in the following sections.

### 3.1.3 $N_2$ Adsorption and Desorption

The textural properties of zeolite-supported nickel oxide and molybdenum oxide catalysts were evaluated from $N_2$ adsorption and desorption.

BET specific surface area, pore volume, and average pore diameter of nickel oxide catalysts are listed in Table 2. The NiO/HMCM-56 sample shows the largest BET area of 374 $m^2\ g^{-1}$ while the BET area of the NiO/HL sample is only 97 $m^2\ g^{-1}$. And other catalysts also have large BET area (>240 $m^2\ g^{-1}$). With regard to pore volume, the maximum is attributed to the NiO/HMCM-56 sample while the NiO/HL sample shows the minimum pore volume. It can be found that the average mesopore diameter of above NiO catalysts differs greatly while the average micropore diameter varying from 0.87 to 1.0 nm differs a little. The NiO/HMCM-56 sample shows the maximal mesopore diameter and micropore diameter, whereas the NiO/HZSM-5 sample is just the opposite.

As displayed in Table 3, the comparison results for textural properties of different molybdenum oxide catalysts exhibit a similarity to those of nickel oxide catalysts because the same zeolites were employed as supports. Concerning specific surface area and pore volume, the maximal values are both attributed to the $MoO_3$/HMCM-56 sample (387 $m^2\ g^{-1}$ and 1.104 $cm^3\ g^{-1}$) while the $MoO_3$/HL sample displays the minimum. For mesopore diameter and micropore diameter, an analogical variability is found and the $MoO_3$/HZSM-5 sample shows the minimum values in both items.

### 3.1.4 FTIR Spectrum of Adsorbed Pyridine and $NH_3$-TPD

The acid type, the acid strength, and the acid amount of zeolite-supported nickel oxide and molybdenum oxide catalysts were determined by means of FTIR spectrum of adsorbed pyridine and $NH_3$-TPD.

Table 4 lists the results of FTIR spectrum of adsorbed pyridine for nickel oxide catalysts under different desorption temperatures (100, 200, 250, and 300 °C). For the NiO/HZSM-5 and NiO/HL samples, only Lewis acid sites are found and determined, and few Brønsted acid sites exist in them. Lewis acid sites and Brønsted acid sites both exist in

**Table 2** Textural properties of zeolite-supported nickel oxide catalysts

| Catalyst | BET specific surface area ($m^2\ g^{-1}$) | Pore volume ($cm^3\ g^{-1}$) | | | Average pore diameter (nm) | |
|---|---|---|---|---|---|---|
| | | Mesopore | Micropore | Total | Mesopore | Micropore |
| NiO/HZSM-5 | 246 | 0.16 | 0.070 | 0.23 | 6.44 | 0.87 |
| NiO/HL | 97 | 0.13 | 0.022 | 0.152 | 8.27 | 0.99 |
| NiO/H$\beta$ | 357 | 0.13 | 0.13 | 0.26 | 7.12 | 0.93 |
| NiO/HMCM-22 | 331 | 0.37 | 0.10 | 0.47 | 12.88 | 0.92 |
| NiO/HMCM-56 | 374 | 0.96 | 0.074 | 1.034 | 16.96 | 1.00 |

**Table 3** Textural properties of zeolite-supported molybdenum oxide catalysts

| Catalyst | BET specific surface area ($m^2\ g^{-1}$) | Pore volume ($cm^3\ g^{-1}$) | | | Average pore diameter (nm) | |
|---|---|---|---|---|---|---|
| | | Mesopore | Micropore | Total | Mesopore | Micropore |
| $MoO_3$/HZSM-5 | 284 | 0.27 | 0.054 | 0.324 | 6.65 | 0.79 |
| $MoO_3$/HL | 96 | 0.14 | 0.010 | 0.150 | 8.04 | 1.07 |
| $MoO_3$/H$\beta$ | 330 | 0.17 | 0.11 | 0.28 | 9.03 | 0.82 |
| $MoO_3$/HMCM-22 | 341 | 0.41 | 0.10 | 0.51 | 15.89 | 0.85 |
| $MoO_3$/HMCM-56 | 387 | 1.04 | 0.064 | 1.104 | 17.73 | 0.96 |

**Table 4** Results of FTIR spectrum of adsorbed pyridine for zeolite-supported nickel oxide catalysts under different desorption temperatures

| Catalyst | Acid amount ($\times 10^{-2}$ mg$^{-1}$) | | | | | | | |
|---|---|---|---|---|---|---|---|---|
| | 100 °C | | 200 °C | | 250 °C | | 300 °C | |
| | Brønsted | Lewis | Brønsted | Lewis | Brønsted | Lewis | Brønsted | Lewis |
| NiO/HZSM-5 | – | 8.4 | – | 4.7 | – | 3.5 | – | 2.8 |
| NiO/HL | – | 8.5 | – | 3.8 | – | 2.2 | – | 2.1 |
| NiO/H$\beta$ | 6.0 | 48.8 | 7.9 | 30.8 | 7.4 | 26.1 | 6.5 | 23.0 |
| NiO/HMCM-22 | 3.4 | 26.8 | 4.1 | 14.6 | 4.2 | 11.7 | 3.9 | 10.0 |
| NiO/HMCM-56 | 5.7 | 18.9 | 4.1 | 12.2 | 3.2 | 10.2 | 2.0 | 8.0 |

the NiO/H$\beta$, NiO/HMCM-22, and NiO/HMCM-56 samples with Brønsted acid sites less than Lewis acid sites. Moreover, the amount of Lewis acid sites decreases in the order: NiO/H$\beta$ > NiO/HMCM-22 > NiO/HMCM-56 > NiO/HZSM-5 > NiO/HL, and the amount of Brønsted acid sites decreases in the order: NiO/H$\beta$ > NiO/HMCM-22 > NiO/HMCM-56. For the NiO/HZSM-5 and NiO/HL samples, the amount of Lewis acid sites decreases gradually with the desorption temperature rising, and the presence of a few Lewis acid sites can still be observed when the desorption temperature reaches 300 °C, which indicates that a few medium or strong Lewis acid sites exist in them besides weak Lewis acid sites. With the desorption temperature rising, the amount of Lewis acid sites and Brønsted acid sites in the NiO/H$\beta$, NiO/HMCM-22, and NiO/HMCM-56 samples also shows a tendency to decrease. And similarly, it is indicated that besides weak Brønsted acid sites and Lewis acid sites, medium or strong Brønsted acid sites and Lewis acid sites exist in these three catalysts.

From the $NH_3$-TPD profiles (Fig. 5), for the NiO/HZSM-5 and NiO/HL samples, a desorption peak appears at 215 and 194 °C, respectively, which indicates that weak acid sites exist in both catalysts. Furthermore, their profiles descend gently and the tailing phenomenon can be observed in the range of 250–400 °C, which shows the presence of overlap of some desorption peaks. And consequently, medium acid sites exist in them besides weak acid sites. There are two main desorption peaks in each profile for the NiO/H$\beta$, NiO/HMCM-22, and NiO/HMCM-56 samples. The low temperature desorption peak is located at 191, 198, and 207 °C, respectively, corresponding to the weak acid sites, whereas the high temperature desorption peak appears at 523, 510, and 500 °C, respectively, corresponding to the strong acid sites. In addition, according to the areas of desorption peaks, the amount of weak acid sites decreases in the order: NiO/H$\beta$ > NiO/HMCM-22 > NiO/HMCM-56 > NiO/HZSM-5 > NiO/HL and the amount of strong acid sites decreases in the order: NiO/H$\beta$ > NiO/HMCM-22 > NiO/HMCM-56. All these results are in accordance with those from FTIR spectrum of adsorbed pyridine.

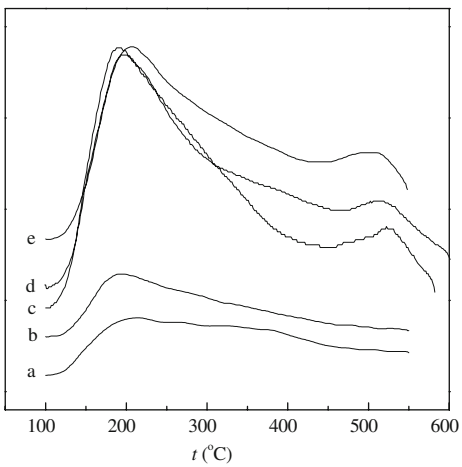


**Fig. 5** $NH_3$-TPD profiles of zeolite-supported nickel oxide catalysts: (*a*) NiO/HZSM-5; (*b*) NiO/HL; (*c*) NiO/H$\beta$; (*d*) NiO/HMCM-22 and (*e*) NiO/HMCM-56

The results of FTIR spectrum of adsorbed pyridine for molybdenum oxide catalysts under different desorption temperatures (100, 200, 250, and 300 °C) are given in Table 5. Lewis acid sites exist in the $MoO_3$/HZSM-5 and $MoO_3$/HL samples, whereas Brønsted acid sites in them are too few to be measured. For the $MoO_3$/H$\beta$, $MoO_3$/HMCM-22, and $MoO_3$/HMCM-56 samples, both Lewis acid sites and Brønsted acid sites can be found and measured. Furthermore, the amount of Lewis acid sites decreases in the order: $MoO_3$/H$\beta$ > $MoO_3$/HMCM-56 > $MoO_3$/HMCM-22 > $MoO_3$/HZSM-5 > $MoO_3$/HL, and the amount of Brønsted acid sites decreases in the order: $MoO_3$/H$\beta$ > $MoO_3$/HMCM-56 > $MoO_3$/HMCM-22. With the desorption temperature increasing, the amount of Lewis acid sites in the $MoO_3$/HZSM-5 and $MoO_3$/HL samples decreases gradually, and the presence of a few Lewis acid sites can still be observed with the desorption carried out at 300 °C, which indicates that a few medium or strong Lewis acid sites exist in them besides weak Lewis acid sites. For the $MoO_3$/H$\beta$, $MoO_3$/HMCM-22, and $MoO_3$/HMCM-56 samples, the amount of Lewis acid sites and Brønsted acid sites also decreases with the desorption temperature

**Table 5** Results of FTIR spectrum of adsorbed pyridine for zeolite-supported molybdenum oxide catalysts under different desorption temperatures

| Catalyst | Acid amount ($\times 10^{-2}$ mg$^{-1}$) | | | | | | | |
|---|---|---|---|---|---|---|---|---|
| | 100 °C | | 200 °C | | 250 °C | | 300 °C | |
| | Brønsted | Lewis | Brønsted | Lewis | Brønsted | Lewis | Brønsted | Lewis |
| $MoO_3$/HZSM-5 | – | 4.7 | – | 3.5 | – | 3.1 | – | 2.9 |
| $MoO_3$/HL | – | 3.0 | – | 1.4 | – | 1.2 | – | 1.0 |
| $MoO_3$/H$\beta$ | 7.4 | 32.2 | 10.2 | 15.0 | 9.9 | 12.4 | 8.7 | 11.3 |
| $MoO_3$/HMCM-22 | 7.3 | 9.0 | 6.4 | 5.2 | 5.7 | 4.0 | 4.5 | 3.4 |
| $MoO_3$/HMCM-56 | 8.8 | 20.6 | 8.7 | 10.4 | 8.6 | 9 | 7.7 | 8.3 |

increasing. And similarly, it is indicated that besides weak Brønsted acid sites and Lewis acid sites, medium or strong Brønsted acid sites and Lewis acid sites exist in them.

Figure 6 shows the $NH_3$-TPD results for zeolite-supported molybdenum oxide catalysts. For all five catalysts, a desorption peak appears at about 190 °C, which indicates that weak acid sites exist in these catalysts and the strength of weak acid sites differs little from each other. Moreover, their $NH_3$-TPD profiles descend gently and the tailing phenomenon occurs in the range of 300–400 °C, which shows the presence of overlap of some desorption peaks. So it can be ascertained that medium acid sites exist in them besides weak acid sites, and the strength of medium acid sites also differs little. According to the areas of desorption peaks, the total acid amount decreases in the order: $MoO_3$/H$\beta$ > $MoO_3$/HMCM-56 > $MoO_3$/HMCM-22 > $MoO_3$/HZSM-5 > $MoO_3$/HL, in accordance with that from FTIR spectrum of adsorbed pyridine.

The comparison results for the acidity between zeolite-supported nickel oxide catalysts and corresponding molybdenum oxide catalysts indicate that nickel oxide catalysts have more Lewis acid sites, whereas molybdenum oxide catalysts have more Brønsted acid sites, and the total acid amount of nickel oxide catalysts is larger. With respect to the acid strength, nickel oxide catalysts exhibit stronger acidity than molybdenum oxide catalysts.

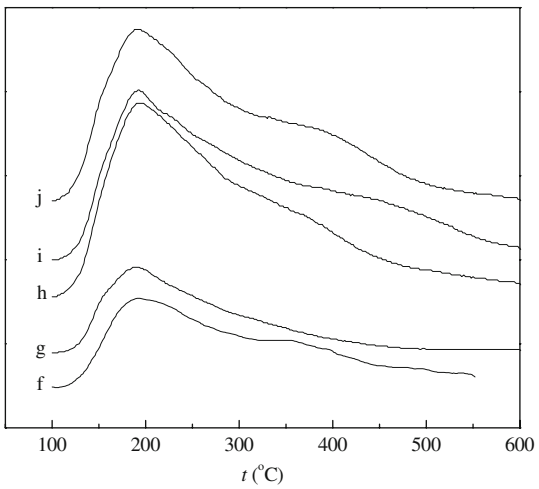


**Fig. 6** $NH_3$-TPD profiles of zeolite-supported molybdenum oxide catalysts: (*f*) $MoO_3$/HZSM-5; (*g*) $MoO_3$/HL; (*h*) $MoO_3$/H$\beta$; (*i*) $MoO_3$/HMCM-22 and (*j*) $MoO_3$/HMCM-56

## 3.2 Hydrodealkylation of $C_9^+$ Heavy Aromatics

### *3.2.1 Catalytic Performance of Zeolite-Supported Nickel Oxide Catalysts*

Our main objective is to investigate the effect of different zeolites on their catalytic performance in hydrodealkylation of commercial $C_9^+$ heavy aromatics. Thus the catalytic activity of zeolite-supported nickel oxide catalysts and corresponding naked zeolites was evaluated as shown in Fig. 7.

It can be found that the employed naked zeolites all exhibit certain catalytic activity when no NiO is loaded. And HZSM-5, HMCM-22, and HMCM-56 have relatively higher activity compared with HL and H$\beta$. When NiO is loaded, the catalytic performance of each zeolite-supported catalyst improves greatly, which indicates that the active component of NiO is quite in favor of promoting the hydrodealkylation process. Five nickel oxide catalysts differ greatly in the catalytic performance. The NiO/H$\beta$ sample exhibits the highest conversion of $C_9^+$ aromatics of 80.68 mol% and the NiO/HMCM-56 sample takes second place with the conversion of 76.2 mol%. For the NiO/HMCM-22 and NiO/HMCM-56 samples, the selectivity of BTX is both more than 80 mol% and exceeds markedly compared with other samples. And the NiO/HMCM-22 sample shows the highest selectivity of BTX of 82.26 mol%. Furthermore, the NiO/HMCM-56 sample exhibits the highest yield of BTX of 61.33 mol%, whereas the yield of BTX for the NiO/HL sample is only 6.21 mol%.

Table 6 lists the product distribution of hydrodealkylation over nickel oxide catalysts. Hydrodealkylation of $C_9^+$ aromatics can produce methane, ethane, propane and etc.

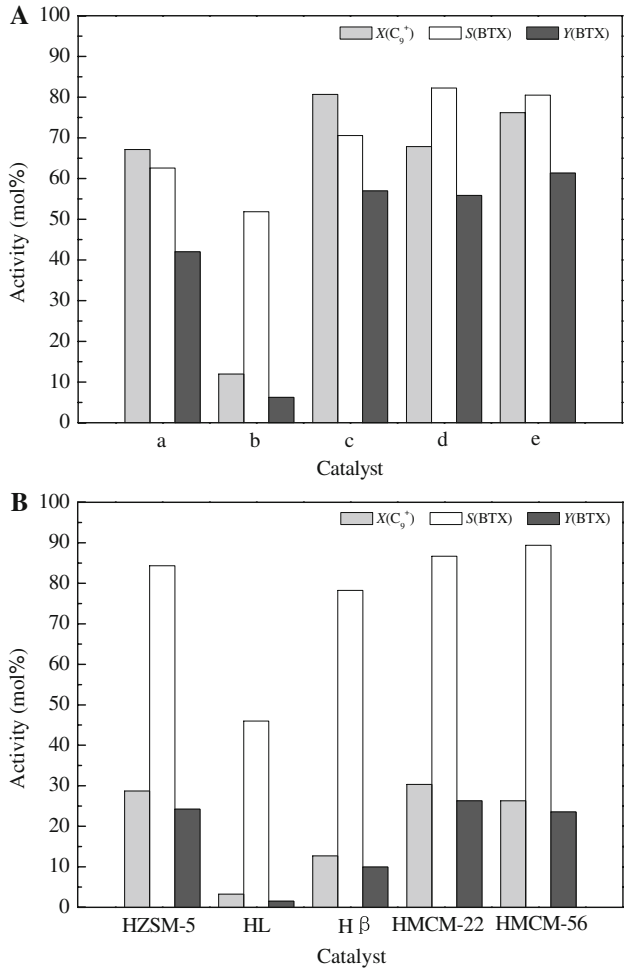


**Fig. 7** Catalytic activity of zeolite-supported nickel oxide catalysts (**a**) and corresponding naked zeolites (**b**) in hydrodealkylation of $C_{9\pm}$ heavy aromatics: (*a*) NiO/HZSM-5; (*b*) NiO/HL; (*c*) NiO/H$\beta$; (*d*) NiO/HMCM-22 and (*e*) NiO/HMCM-56. Reaction conditions were: $t$ = 460 °C, $p$ = 3 MPa, WHSV = 3.62 $h^{-1}$, $V(H_2)$:$V(C_{9\pm})$ = 1,600

So the weight of liquid product decreases to a certain extent compared with the heavy aromatics feed, i.e., the yield of liquid product is less than 100 wt%. Although the NiO/H$\beta$ sample shows the highest conversion of $C_9^+$ aromatics, its yield of liquid product is too low and only 66.76 wt%. For the NiO/HMCM-22 and NiO/HMCM-56 samples, their yield of liquid product is as high as above 75 wt%, whereas the NiO/HL sample exhibits the highest yield of liquid product due to its lowest activity. The formation of ethylbenzene (EB) is not expected, since the presence of EB in the *p*-xylene recovery unit strongly reduces the operating efficiency due to the small difference in boiling point between EB and *p*-xylene, and this can create a bottleneck in the production of xylenes in an industrial plant [18]. Among above five catalysts, only the employment of NiO/HL causes the formation of EB. Furthermore, the highest mass yield of xylenes of 29.72 wt% can be obtained when the NiO/HMCM-56 sample is used.

To sum up, among five zeolite-supported nickel oxide catalysts, the NiO/HMCM-56 sample exhibits the best catalytic performance in hydrodealkylation of $C_9^+$ heavy aromatics with the high conversion of $C_9^+$ aromatics, the high selectivity of BTX and the highest yield of BTX, and its mass yield of xylenes also exceeds.

### 3.2.2 *Catalytic Performance of Zeolite-Supported Molybdenum Oxide Catalysts*

Figure 8 displays the catalytic results of different zeolites with no $MoO_3$ loaded and impregnated with $MoO_3$. Compared with the data shown in Fig. 7b, the catalytic activity of each naked zeolite (Fig. 8b) increases greatly with the reaction temperature rising from 460 to 550 °C. When $MoO_3$ is loaded, the catalytic performance of each zeolite-supported catalyst improves obviously, which shows that $MoO_3$ can also promote the hydrodealkylation process. It can be also seen that different zeolites influence the catalytic performance greatly. The highest conversion of $C_9^+$ aromatics of 95.51 mol% occurs over the $MoO_3$/H$\beta$ sample, and the $MoO_3$/HMCM-56 sample takes second place. The $MoO_3$/H$\beta$ sample shows the lowest selectivity of BTX of 62.88 mol%, and other four samples differ little with their selectivity of BTX all more than 82 mol%. In

**Table 6** Product distribution of hydrodealkylation of $C_9^+$ heavy aromatics over zeolite-supported nickel oxide catalysts

| Catalyst | Composition of products (wt%) | | | | | | | | *m*(liquid product):*m*(feed) (wt%) |
|---|---|---|---|---|---|---|---|---|---|
| | B | T | X | Ethylbenzene | $C_8^{-a}$ | $C_9$ | $C_{10}$ | $C_{10}^+$ | |
| NiO/HZSM-5 | 7.28 | 15.26 | 27.14 | 0 | 0.55 | 37.05 | 12.40 | 0.32 | 64.90 |
| NiO/HL | 0 | 0.91 | 4.57 | 0.55 | 0 | 60.87 | 30.47 | 2.62 | 93.15 |
| NiO/H$\beta$ | 5.08 | 23.32 | 38.21 | 0 | 5.24 | 23.89 | 4.19 | 0 | 66.76 |
| NiO/HMCM-22 | 2.95 | 16.25 | 36.48 | 0 | 4.88 | 31.63 | 7.50 | 0.31 | 79.56 |
| NiO/HMCM-56 | 3.51 | 20.93 | 38.95 | 0 | 6.32 | 25.62 | 4.67 | 0 | 76.30 |

Reaction conditions were: $t$ = 460 °C, $p$ = 3 MPa, WHSV = 3.62 $h^{-1}$, $V(H_2)$:$V(C_9^+)$ = 1,600

[a] Paraffins and naphthenes with number of carbon atoms below eight

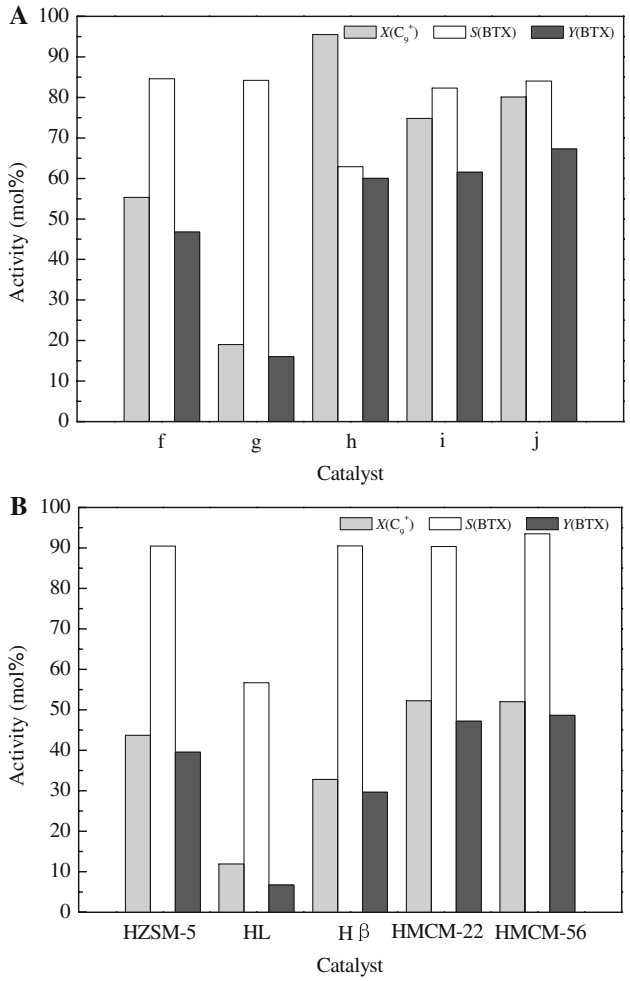


**Fig. 8** Catalytic activity of zeolite-supported molybdenum oxide catalysts (**a**) and corresponding naked zeolites (**b**) in hydrodealkylation of $C_{9\pm}$ heavy aromatics: (*f*) $MoO_3$/HZSM-5; (*g*) $MoO_3$/HL; (*h*) $MoO_3/H\beta$; (*i*) $MoO_3$/HMCM-22 and (*j*) $MoO_3$/HMCM-56. Reaction conditions were: $t$ = 550 °C, $p$ = 3 MPa, WHSV = 3.62 $h^{-1}$, $V(H_2):V(C_{9\pm})$ = 1,600

addition, the $MoO_3$/HMCM-56 sample exhibits the highest yield of BTX of 67.3 mol%, whereas the yield of BTX for the $MoO_3$/HL sample is only 16.01 mol%.

As shown in Table 7, the $MoO_3/H\beta$ sample exhibits the lowest yield of liquid product of 50.63 wt% despite its highest conversion of $C_9^+$ aromatics. And then the $MoO_3$/HL sample exhibits the highest yield of liquid product due to its lowest activity. EB is not found in the liquid products when the molybdenum oxide catalysts are employed, except the $MoO_3/H\beta$ and $MoO_3$/HL samples. In addition, similar to the NiO/HMCM-56 sample, the HMCM-56 zeolite impregnated with molybdenum oxide also exhibits the highest mass yield of xylenes of 29.75 wt%.

So on the whole, the $MoO_3$/HMCM-56 sample also shows the best performance among the zeolite-supported molybdenum oxide catalysts like the NiO/HMCM-56 sample.

## 3.3 Effect of Different Zeolites on the Catalytic Performance

In this section, the effect of different zeolites on the catalytic performance, i.e., the correlation between the structural properties and acidity of the zeolite-supported catalysts and their catalytic activity, was further discussed.

### *3.3.1 Specific Surface Area and Pore Structure*

Characterization results of $N_2$ adsorption and desorption indicate that whether zeolite-supported nickel oxide catalysts or zeolite-supported molybdenum oxide catalysts differ greatly in specific surface area and pore structure. According to the catalytic results shown in Figs. 7 and 8, it can be concluded that the specific surface area of different zeolites impregnated with nickel oxide or molybdenum oxide influences the conversion of $C_9^+$ aromatics greatly. And with the specific surface area increasing, the conversion of $C_9^+$ aromatics shows a tendency to increase. But the pore diameter has little effect on the catalytic performance. Though the catalysts with HZSM-5 as support have the minimum pore diameter, their conversion of $C_9^+$ aromatics is not the least. And the pore diameter of H$\beta$-supported catalysts is not the maximum, but their conversion of $C_9^+$ aromatics exceeds compared with other catalysts.

**Table 7** Product distribution of hydrodealkylation of $C_9^+$ heavy aromatics over zeolite-supported molybdenum oxide catalysts

| Catalyst | Composition of products (wt%) | | | | | | | | *m*(liquid product):*m*(feed) (wt%) |
|---|---|---|---|---|---|---|---|---|---|
| | B | T | X | Ethylbenzene | $C_8^{-a}$ | $C_9$ | $C_{10}$ | $C_{10}^+$ | |
| $MoO_3$/HZSM-5 | 3.18 | 13.86 | 28.18 | 0.00 | 0.44 | 39.60 | 10.59 | 4.15 | 81.42 |
| $MoO_3$/HL | 0.43 | 2.48 | 10.89 | 0.75 | 0.00 | 54.96 | 28.88 | 1.60 | 94.21 |
| $MoO_3/H\beta$ | 18.34 | 41.11 | 27.81 | 0.53 | 3.56 | 7.51 | 0.62 | 0.51 | 50.63 |
| $MoO_3$/HMCM-22 | 5.22 | 21.00 | 38.73 | 0.00 | 1.83 | 26.73 | 5.19 | 1.29 | 74.19 |
| $MoO_3$/HMCM-56 | 5.33 | 25.54 | 40.35 | 0.00 | 2.52 | 22.12 | 3.50 | 0.64 | 73.74 |

Reaction conditions were: $t$ = 550 °C, $p$ = 3 MPa, WHSV = 3.62 $h^{-1}$, $V(H_2):V(C_9^+)$ = 1,600

[a] Paraffins and naphthenes with number of carbon atoms below eight

### 3.3.2 Acidity

As previously mentioned in Sect. 3.1.4, zeolite-supported nickel oxide or molybdenum oxide catalysts exhibit different acidity. In the case of nickel oxide catalysts, the NiO/H$\beta$, NiO/HMCM-22, and NiO/HMCM-56 samples all have strong Brønsted acid sites, strong Lewis acid sites, weak Brønsted acid sites, and weak Lewis acid sites, whereas the NiO/HZSM-5 and NiO/HL samples only have medium Lewis acid sites and weak Lewis acid sites. Correlating these acidity results with their catalytic performance (Fig. 7), we can find that the conversion of $C_9^+$ aromatics for the NiO/H$\beta$, NiO/HMCM-22, and NiO/HMCM-56 samples is remarkably higher than that for other two samples because they have the advantage of acid type, stronger acid strength and more acid amount mentioned above. Among five nickel oxide catalysts, the NiO/H$\beta$ sample exhibits the presence of Brønsted acid sites, the strongest acid strength and the maximal acid amount, so it can be deduced that this sample shows the highest conversion of $C_9^+$ aromatics, which is just in accordance with the experimental results. Therefore, the presence of Brønsted acid sites, the growth of the strength of Lewis acid sites and the increase of acid amount can all enhance the conversion of $C_9^+$ aromatics.

With regard to molybdenum oxide catalysts, medium Brønsted acid sites, medium Lewis acid sites, weak Brønsted acid sites, and weak Lewis acid sites exist in the $MoO_3$/H$\beta$, $MoO_3$/HMCM-56, and $MoO_3$/HMCM-22 samples, whereas only medium Lewis acid sites and weak Lewis acid sites exist in the $MoO_3$/HZSM-5 and $MoO_3$/HL samples. Then according to the experimental results (Fig. 8), an identical conclusion is also drawn that the presence of Brønsted acid sites and the increase of acid amount can both improve the conversion of $C_9^+$ aromatics. And this is confirmed by the high conversion of $C_9^+$ aromatics for the $MoO_3$/H$\beta$ sample.

In the work of Toppi [19], the mechanisms of *n*-propylbenzene hydrodealkylation reactions over $Al_2O_3$ and 1 wt% Cl–$Al_2O_3$ catalysts with different acid sites were studied. It was reported that benzene is formed on strong Brønsted acid sites via a carbocationic pathway and isomerization reactions occur on weak Brønsted acid sites. In addition, toluene and ethylbenzene are formed on strong and weak Lewis acid sites via a radical pathway, respectively. According to Toppi's proposition, whether Brønsted acid sites or Lewis acid sites are both advantageous for the conversion of *n*-propylbenzene, and thus more acid sites will accelerate this process. Though the feed employed in the current work is quite different from Toppi's, our conclusion is in agreement with above deduction.

### 3.3.3 Interaction Between Zeolite and Metal Oxide

From the reduction performance of zeolite-supported nickel oxide catalysts (Fig. 3), the five samples can be classified as three groups: (1) NiO/HZSM-5 and NiO/H$\beta$ with the relatively strong interaction between zeolite and NiO, where a part of nickel species is located in the framework of zeolite and the maximal reduction temperature is beyond 550 °C; (2) NiO/HMCM-56 and NiO/HMCM-22 with the moderate interaction, where the maximal reduction temperature of nickel species occurs at 520–540 °C; and (3) NiO/HL with the relatively weak interaction, where the maximal reduction temperature is less than 520 °C. Correlating the extent of interaction with their catalytic performance (Fig. 7), we can find that the selectivity of BTX is greatly affected by the interaction between zeolite and NiO. The catalysts with the moderate interaction such as the NiO/HMCM-22 and NiO/HMCM-56 samples exhibit the relatively high selectivity. And the selectivity decreases when the interaction between zeolite and NiO becomes stronger or weaker.

In the case of molybdenum oxide catalysts (Fig. 4), the molybdenum species located in the channels of zeolite and associated with Brønsted acid site exists only in the $MoO_3$/H$\beta$ sample and other four samples do not contain this species. Considering the acidity, the $MoO_3$/H$\beta$ sample has the most Brønsted acid sites and the highest density of Brønsted acid sites so that the probability of forming the molybdenum species associated with Brønsted acid site is maximal. Correlating the difference in the molybdenum species with their catalytic performance (Fig. 8), we can draw the conclusion that the presence of the molybdenum species associated with Brønsted acid site causes the remarkable reduction of selectivity of BTX, which is the embodiment of the impact of the interaction between zeolite and $MoO_3$ on the catalytic performance. It is possibly because this species could promote the occurrence of some side reactions such as hydrocracking which causes the direct scission of aromatic ring.

## 4 Conclusions

Different zeolites impregnated with nickel oxide or molybdenum oxide exhibit strikingly diverse activity in hydrodealkylation of commercial $C_9^+$ heavy aromatics. It is indicated that the HMCM-56 catalysts show the greatest overall catalytic performance with the yield of BTX more than 60 mol% under experimental conditions, whether using NiO or $MoO_3$ as the active component.

The results from the correlation between the structural properties and acidity of the zeolite-supported catalysts and their catalytic activity reveal that the catalytic

performance is greatly influenced by the specific surface area, the acidity and the interaction between zeolite and metal oxide, but the pore diameter of catalysts has little effect. For zeolite-supported nickel oxide catalysts, the samples with the moderate interaction between zeolite and NiO exhibit the relatively high selectivity. And for zeolite-supported molybdenum oxide catalysts, the presence of the molybdenum species located in the channels of zeolite and associated with Brønsted acid site causes the remarkable reduction of selectivity of BTX. The acidity and the specific surface area have a direct impact on the conversion of $C_9^+$ aromatics. With the specific surface area increasing, the conversion of $C_9^+$ aromatics shows a tendency to increase. The presence of Brønsted acid sites, the growth of the strength of Lewis acid sites and the increase of acid amount can all enhance the conversion of $C_9^+$ aromatics, whether using NiO or $MoO_3$ as the active component.

**Acknowledgments** The authors thank China National Petroleum Corporation (CNPC) (Project W06-04A-01-01A) for the financial support of this work.

## References

1. Grenoble DC (1979) J Catal 56:32
2. Ozawa A, Kubota T, Mie H, Taketani T (1976) JP 51,029,131
3. Daly FP, Wilhelm FC (1984) USP 4,436,836
4. Wu AH, Drake CA (1998) USP 5,789,642
5. Wu AH, Drake CA, Melton RJ (1998) USP 5,714,660
6. Tabak SA, Morrison RA (1982) USP 4,341,622
7. Howley PA, Shih SS (1991) USP 5,001,296
8. Wu AH, Drake CA (1997) USP 5,698,757
9. Kato H, Tanaka H, Iwayama K, Ichioka R (1998) EP 0,816,311
10. Ichioka R, Yamakawa S, Okino H, Kato H, Iwayama K, Konta H, Kitamura A (2000) USP 6,040,490
11. Serra JM, Guillon E, Corma A (2004) J Catal 227:459
12. McMinn TE, Stachelczyk DA (2005) USP 2,005,065,017
13. Choi S, Oh SH, Kim YS, Seong KH, Lim BS, Lee JH (2006) Catal Surv Asia 10:110
14. Pawelec B, Mariscal R, Navarro RM, Campos-Martin JM, Fierro JLG (2004) Appl Catal A 262:155
15. Fúnez A, De Lucas A, Sánchez P, Ramos MJ, Valverde JL (2008) Chem Eng J 136:267
16. Arnoldy P, De Jonge JCM, Moulijn JA (1985) J Phys Chem 89:4517
17. Liu H, Xu Y (2006) Chin J Catal 27:319
18. Serra JM, Guillon E, Corma A (2005) J Catal 232:342
19. Toppi S, Thomas C, Sayag C (2002) J Catal 210:431